RAA 2015 Vol. **15** No. **11**, 1893–1904 doi: 10.1088/1674–4527/15/11/011
http://www.raa-journal.org *http://www.iop.org/journals/raa*

Research in Astronomy and Astrophysics

Laboratory verification of the Active Particle-induced X-ray Spectrometer (APXS) on the Chang'e-3 mission

Guang-Liang Zhang[1,2], Chun-Lai Li[1,2], Xiao-Hui Fu[1,2], Li-Yan Zhang[1,2], Cao Ban[1,2], Han Li[1,2], Yong-Liao Zou[1,2], Wen-Xi Peng[3], Xing-Zhu Cui[3], Cheng-Mo Zhang[3] and Huan-Yu Wang[3]

[1] National Astronomical Observatories, Chinese Academy of Sciences, Beijing 100012, China; *zhanggl@nao.cas.cn*
[2] Key Laboratory of Lunar and Deep Space Exploration, National Astronomical Observatories, Chinese Academy of Sciences, Beijing 100012, China
[3] Institute of High Energy Physics, Chinese Academy of Sciences, Beijing 100049, China

Received 2014 July 22; accepted 2015 April 17

Abstract In the Chang'e-3 mission, the Active Particle-induced X-ray Spectrometer (APXS) on the Yutu rover is used to analyze the chemical composition of lunar soil and rock samples. APXS data are only valid are only if the sensor head gets close to the target and integration time lasts long enough. Therefore, working distance and integration time are the dominant factors that affect APXS results. This study confirms the ability of APXS to detect elements and investigates the effects of distance and time on the measurements. We make use of a backup APXS instrument to determine the chemical composition of both powder and bulk samples under the conditions of different working distances and integration times. The results indicate that APXS can detect seven major elements, including Mg, Al, Si, K, Ca, Ti and Fe under the condition that the working distance is less than 30 mm and having an integration time of 30 min. The statistical deviation is smaller than 15%. This demonstrates the instrument's ability to detect major elements in the sample. Our measurements also indicate the increase of integration time could reduce the measurement error of peak area, which is useful for detecting the elements Mg, Al and Si. However, an increase in working distance can result in larger errors in measurement, which significantly affects the detection of the element Mg.

Key words: major elements: working distance — integration time — APXS: Chang'e-3 mission

1 INTRODUCTION

For a lunar (See Fu et al. 2014) or planetary mission, the Alpha Particle-induced X-ray spectrometer (APXS) is the most important instrument on the rover or lander that is used to analyze the chemical composition of soils and rocks. These kinds of instruments have been widely used in the Surveyor series of lunar missions, three generations of Mars rovers (Mars Pathfinder, Spirit and Opportunity, and Curiosity), and the British Beagle 2 lander because of their small size, low power consumption

and easy sample preparation. The APXS sensor head is always mounted on the turret of the rover's robotic arm, which makes it easier to detect the soils and rocks of interest in a rover's path.

The Surveyor 5 mission was the first to conduct in-situ chemical analysis of the lunar surface with an alpha-scattering instrument based on Rutherford's alpha-particle scattering theory (Economou 2011). The successful application of this technique has also been utilized to explore Mars. Each Viking lander carried an X-Ray Fluorescence Spectrometer (XRFS) to perform elemental analysis of the Martian regolith, using ^{55}Fe and ^{109}Cd as radioactive sources. Detectable elements range from Na ($Z = 11$) to Nb ($Z = 41$). Probes that were part of the Venera and Vega programs analyzed major rock-forming elements by X-ray fluorescence (XRF) with the radioactive sources ^{238}Pu and ^{55}Fe.

Three generations of Mars rovers all carried an APXS-type instrument using the radioactive source ^{244}Cm as part of the science payload. The APXS on the Sojourner rover had three instrumental modes (Economou 2001). The α-mode measured the energy and intensity of back-scattered α-particles from a sample, which enabled measurement of all major and some minor rock-forming elements, except for hydrogen. The proton-mode measured the intensity of protons emitted from (α, p) reactions in the sample, which enabled measurement of the elements Na, Mg, Al, Si, S and N. The X-ray mode measured the intensities of X-rays produced from α-particles and X-rays striking the sample and enabled measurement of abundances of elements that have X-ray energies ranging from 1 to 15 keV. This enabled measurements of major and minor rock-forming elements ranging in atomic number from Na through Ni. The α-mode was also called Rutherford backscattering (RBS) while the third was Particle Induced X-ray Emission (PIXE) and XRF. Unlike the Pathfinder mission, APXSs on the Spirit and Opportunity rovers of the Mars Exploration mission (MER) did not have a proton mode. The elements detected by MER APXS in rock and soil were typically Mg, Al, Si, K, Ca, Fe and trace elements (Na, P, S, Cl, Ti, Cr) (Rieder et al. 2003; Gellert et al. 2006). APXS on the Mars Science Laboratory (MSL) Curiosity rover was an advanced version of its predecessor instrument developed for the MER mission. It employed XRF and particle-induced X-ray emission (PIXE), based on intense ^{244}Cm radionuclide sources, to conduct elemental analysis of Martian soils and rocks. For the ESA Rosetta mission, the APXS is improved based on the instrument onboard the Mars Pathfinder to provide basic compositional data about the comet's surface.

In general, the elemental composition from the X-ray data and associated least-squares fitting programs can be derived by the fundamental parameter approach that has been used to reduce alpha and proton data (Economou 2001; Gellert et al. 2006). A new fundamental parameter approach was used by Campbell et al. (2009, 2010) and it employed a spectral fitting code, GUAPX. The PIXE analysis software package GUPIX added the capability of manual simultaneous XRF analysis. The observed yield $Y(Z)$ of a specific characteristic X-ray of a given element (atomic number Z, concentration C_Z) in an APXS measurement with duration T seconds can be described by the equation

$$Y(Z) = H \cdot C_Z \cdot T \cdot k(Z) \cdot [Y_{1,\mathrm{PIXE}}(Z, M) + \sum Y_{1,\mathrm{XRF}}(Z, M)] \cdot t_Z \cdot \varepsilon_Z \,, \qquad (1)$$

where $Y_1(Z, M)$ can be computed theoretically by the X-ray yield from element Z per unit concentration within a defined matrix M, per steradian of solid angle, per ion or photon. $Y_{1,\mathrm{PIXE}}(Z, M)$ represents X-rays from the PIXE process arising from the alpha particles emitted by the APXS excitation source (^{244}Cm) and $Y_{1,\mathrm{XRF}}(Z, M)$ represents X-rays from the XRF process arising from plutonium L X-rays from the source. t_Z is the X-ray transmission fraction through any material interposed between the detector and the surface of a sample. ε_Z is the intrinsic efficiency of the detector and its value for iron K X-rays is close to 1.0. H is the single instrumental calibration factor and can be determined in the calibration exercise. $k(Z)$ is an experimentally determined corrective function and it has values slightly different from a default value of 1.0.

In this study the GUAPX code has been used to analyze APXS spectra of MER and MSL. Then, the fundamental parameter approach is applied to convert the intensities to elemental concentrations.

The third Chinese lunar mission, Chang'e-3 (CE-3), successfully landed on the Moon on 2013 December 14 (Ip et al. 2014). The landing site of CE-3 was located at the northern part of Mare Imbrium, which is quite close to the boundary of two disparate geological units (Li et al. 2014; Liu et al. 2014b; Ren et al. 2014). APXS was mounted on the rover's robotic arm and began operating on the Moon. APXS's scientific objective was to perform an in-situ analysis of the chemical compositions of lunar soils and rocks during the exploration by the rover, named Yutu (Fu et al. 2014; He et al. 2014; Liu et al. 2014a). The APXS spectra were generated via both XRF and PIXE, which is the same process as used by the APXS-type instrument on MSL. Instead of ^{244}Cm, a combination of elements with ^{55}Fe (4×, 70 mCi each) and ^{109}Cd (4×, 2.5 mCi each) was chosen as radioactive sources for the APXS on Yutu (Peng et al. 2014). When X-rays and alpha particles interact with atoms in a surface material, they knock electrons out of their orbits, producing an energy release by emitting X-rays that can be measured with a silicon drift detector. An element and its concentration can be identified by analyzing its peak energy and intensity.

In terms of quantitative analysis, the measured X-ray intensities are converted into values representing the concentration of elements. This issue is rather complicated because the measured intensities depend not only on the element concentration but also on matrix effects, sample type (solid, liquid or powder samples), shape and thickness of the analyzed sample, and measurement conditions such as geometrical setup of the spectrometer (Ji et al. 2005; Liang et al. 2013). According to the principle of APXS, the data are only valid if the sensor head gets close to the target and integration time lasts long enough (Tan et al. 2014). Therefore, working distance and integration time in each APXS acquisition are the dominant factors that affect results generated by APXS. Matrix effects and sample shape and thickness are not involved in this study. In order to test the ability of APXS to detect elements and investigate the influence of distance and time, we used a backup APXS instrument to determine the chemical composition of powder and bulk samples with different working distances and integration times.

In this article, Section 2 gives the experiment procedure, Section 3 provides a description of data processing methods used and Section 4 draws conclusions.

2 APXS GROUND TEST

2.1 Experimental Setup

The experiments were carried out at the Institute of High Energy Physics, Chinese Academy of Sciences. The essential facilities include vacuum equipment, a Network Interface Module (NIM) chassis, a DC regulated power supply, a Portable Multi-Channel Analyzer (PMCA), a movable platform with sample stage, and a computer. The measurements were performed in a vacuum. The sensor head was mounted on the movable platform. Then both of them were placed in the vacuum chamber. The NIM bin and DC regulated power supply provided the power to the sensor head. PMCA collected the data and imported them to the computer. The level of radioactivity of the source ^{55}Fe was 300 mCi in May 2013 and the value of ^{209}Cd was 22 mCi in February 2013. On the day that the experiment was conducted (2014 April 24), the levels of radioactivity for ^{55}Fe and ^{209}Cd were 233.8 and 19.4 mCi respectively.

2.2 Sample Preparation

The starting materials were samples of bulk basalt and powder lunar simulant used in these experiments. Cenozoic basalts were picked from Damiao town, Hebei province, China. The size of the bulk basalt sample was $13\times13\times2$ cm^3 (Fig. 1 left). It mostly consisted of plagioclase and pyroxene and contained some magnetite as an accessory mineral that was identified in hand specimens and a thin section of rock.

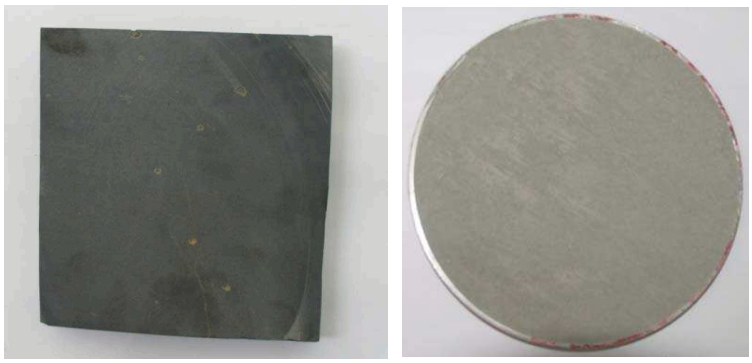

Fig. 1 Bulk basalt (*left*) and powder (*right*) samples used in the present study.

Table 1 Chemical Compositions of the Powder Samples

Institute	Major element concentration (%)									
	Na	Mg	Al	Si	P	K	Ca	Ti	Mn	Fe
Institute of Geophysics and Geology	2.19	5.48	7.17	20.52	0.327	1.68	6.53	1.54	0.132	9.63
Langfang Geo-analysis Center	2.21	5.58	7.16	20.62	0.333	1.69	6.54	1.55	0.135	9.5
Beijing Research Institute of Uranium Geology	2.19	5.45	7.12	20.59	0.336	1.72	6.61	1.56	0.132	9.57
Average	2.2	5.5	7.15	20.58	0.33	1.7	6.56	1.55	0.13	9.57

The powder samples were made of crushed basalt and phosphorous. The median diameter of powdered samples ranged from 40 to 100 μm. The loose powder was packed in a round aluminum container with a planar surface for APXS analysis (Fig. 1 right). Chemical compositions of the powder samples were analyzed by XRFSs in three different institutes and the results are listed in Table 1.

2.3 Experimental Procedures

The APXS sensor head and movable platform were installed in the vacuum chamber (the white object in the middle of Fig. 2). As required, we connected the NIM bin, DC regulated power supply, PMCA and computer. The sample was placed on the sample stage of the movable platform, which could control the distance between the sample and sensor head. The head was normal to the surface of the sample. After the door of the vacuum chamber was closed, the vacuum pumping equipment began operation. When pressure in the chamber dropped to 10 Pa, we could stop pumping and start APXS detection. At the same time, we recorded the time when detections with APXS were made. The counting data could be displayed real-time on the computer. Table 2 lists the working distance and integration time of the bulk basalt and powder samples.

2.4 Data Processing

The first step for APXS data processing is to convert the channel number of each spectrum to X-ray energy (Fig. 3). The temperature of the APXS sensor will vary according to the ambient temperature on the lunar surface (Wu et al. 2012). In order to avoid an inevitable change in the detector response with temperature, a traditional but effective calibration includes a gain (ΔkeV/Channel) that varies as a function of temperature and an offset yielding the relationship. It can be expressed as

$$E = C \cdot G + O\,, \tag{2}$$

Fig. 2 The APXS sensor head and movable platform in the vacuum chamber.

Table 2 The Working Distance and Integration Time of the Powder Samples and Bulk Basalt

	Sample	Working distance (mm)	Integration time (min)
1		30	10
2		30	20
3	Powder samples	30	30
4	with different times	30	45
5		30	60
6		30	90
7		10	30
8		20	30
9	Powder samples	30	30
10	with different working	40	30
11	distances	50	30
12		70	30
13		90	30
14		110	30
15	Bulk basalt	30	30

where E is the energy of a characteristic X-ray from an element, C is the channel number of each spectrum, G is a function of temperature and O is the offset of temperature.

We can pick several well-known peaks in the spectrum and build the relationship between peak center and energy of a characteristic X-ray from an element. The gain and offset can be calculated with the least-squares method.

The second step is the dead time correction (Fig. 3). We can obtain a minimum time when a detector that responds sequentially for individual events requires a minimum amount of time that should separate two events so that these events can be recorded as two separate events. This minimum time is called the “dead time” (Fu et al. 2014). The value of dead time was set in the main electronics unit during development of the instrument. Dead time correction can be calculated with the following equation (Fu et al. 2014)

$$C_1 = \frac{C_0}{8 - t \cdot C_0}, \tag{3}$$

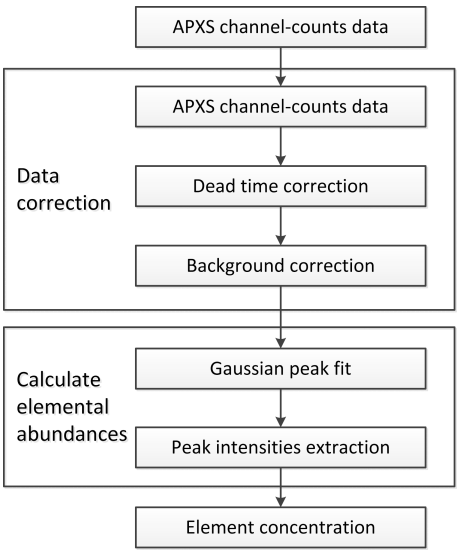

Fig. 3 APXS data processing procedure.

where C_0 is the counts from each channel before dead time correction, C_1 is the counts after correction, and t is the dead time of the APXS detector. Note that t is an engineering parameter that is related to the detector in APXS. Ground engineering software will parse out the parameters displayed on the screen. The value displayed on the interface was 12.5 μs. In order to facilitate the calculation and verification, t was set to 12.5 μs in the test data processing according to the characteristics of the backup APXS instrument.

The third step is background correction (Fig. 3). A background function is usually applied to subtract the background from a spectrum. For narrow peaks, a linear background function can be used. It can be expressed as

$$L(i, B) = b_1 + b_2 i \,, \tag{4}$$

where L is a linear background function for the fitted counts of each channel, i is the channel, and b_1 and b_2 are the slope and intercept of the line respectively. For wide peaks and a nonlinear background, a third order function is used. It can be expressed as

$$L(i, B) = b_1 + b_2 i + b_2 i^2 \,. \tag{5}$$

After the corrections discussed above are applied, we used the Origin program to fit the Gaussian peaks and calculate peak areas as intensities. Then the fundamental parameter approach is applied to convert the intensities to elemental concentrations in Figure 4.

In Figure 4, R_i^{m} is the relative intensity measurement of a component in an unknown sample. It can be expressed as

$$R_i^{\mathrm{m}} = \frac{I_i^{\mathrm{m}}}{I_{i,\mathrm{s}}^{\mathrm{m}}} \,, \tag{6}$$

where I_i^{m} is the intensity measurement of a given component in the unknown sample and $I_{i,\mathrm{s}}^{\mathrm{m}}$ is the intensity measurement of a given component in a standard sample.

In Figure 4, R_i^{cal} is the theoretical value of relative intensity of a given component in the unknown sample. It can be expressed as

$$R_i^{\mathrm{cal}} = \frac{I_i^{\mathrm{cal}}}{I_{i,\mathrm{s}}^{\mathrm{cal}}} \,, \tag{7}$$

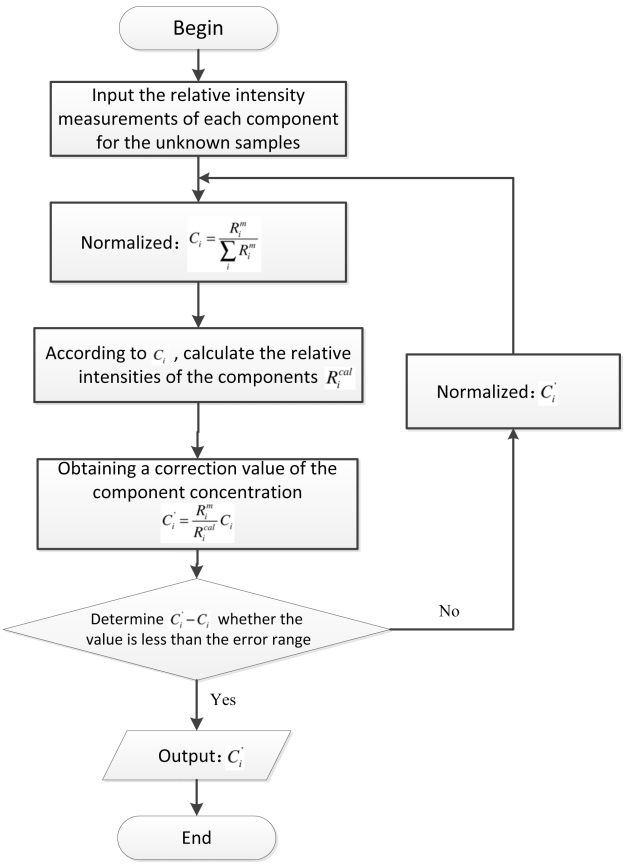

Fig. 4 A flow chart illustrating the fundamental parameter approach for converting the intensities to elemental concentrations.

where I_i^{cal} is the theoretical value of intensity for a given component in the unknown sample and $I_{i,\mathrm{s}}^{\mathrm{cal}}$ is the theoretical value of intensity for a given component in the standard sample.

According to APXS data processing and methods in Figure 4, we analyzed and calculated the APXS test data. Tables 3–6 list the elemental types and concentrations of the test samples. Using the elemental concentrations in Table 1 as standard values, we calculated the statistical deviation and assess the accuracy of APXS analyses. In the study, the statistical deviation is used as the evaluation indicator.

$$D = \left| \frac{A_{\mathrm{APXS}} - A_{\mathrm{stad}}}{A_{\mathrm{stad}}} \right| \times 100\% \,, \tag{8}$$

where D is the relative error, A_{APXS} is the elemental concentration analyzed by APXS, and A_{stad} is the elemental concentration analyzed by XRF in a lab as the reference.

3 RESULTS AND ANALYSIS

3.1 Results of the Powder Samples with Different Integration Times

Figure 5 shows the channel count data of powder samples with different integration times. Seven elements were identified from the spectrum, including Mg, Al, Si, K, Ca, Ti and Fe. We performed

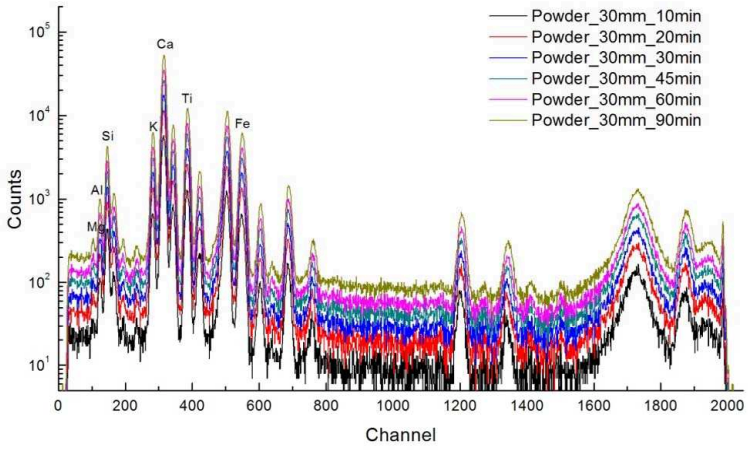

Fig. 5 APXS spectra of the powder samples with different integration times.

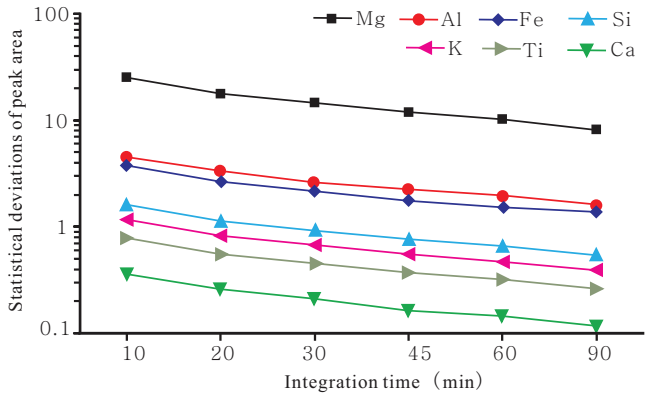

Fig. 6 The statistical deviations of peak area correlated with integration time.

an iterative least-squares fit of a single Gaussian peak and calculated the area of each peak and its statistical deviation.

Table 3 lists the peak areas and statistical deviations of seven elements. To investigate correlations between them, the data are plotted in Figure 6. Note that the statistical deviation decreases as the integration time increases. The peaks of the light elements, Mg, Al and Si, are significantly improved by increasing integration time. This indicates that when APXS works on the Moon, a sufficient integration time is necessary for precise APXS results and it also helps in the identification of light elements Mg, Al and Si. These results verify the linearity of the APXS detector.

The elemental concentrations are obtained using the fundamental parameter approach. Compared with standard values, we found that increasing the integration time showed a different behavior compared to the elemental concentration results. The statistical deviations of Mg concentration under the integration times 10, 20 and 30 min are respectively 13.33%, 14.63% and 0.37% (Table 4). It means that the increase in integration time did improve the accuracy of the detected Mg concentration.

Table 3 Peak Areas and Their Statistical Deviations with Different Integration Times

	Integration time (min)	Mg	Al	Si	K	Ca	Ti	Fe
Peak area (counts)	10	119	853	4643	8240	72217	16859	1291
	20	337	1695	9601	16932	147965	34685	2568
	30	430	3014	14355	25618	223833	52399	4005
	45	651	3679	21578	38425	337489	79153	6173
	60	831	4975	28778	51486	451800	105664	8311
	90	1319	9048	43201	76790	679017	159062	12243
Statistical deviations (%)	10	24.99	4.68	1.61	1.16	0.36	0.78	3.74
	20	17.67	3.31	1.14	0.82	0.26	0.55	2.65
	30	14.43	2.7	0.93	0.67	0.21	0.45	2.16
	45	11.78	2.2	0.76	0.55	0.17	0.37	1.76
	60	10.2	1.91	0.66	0.47	0.15	0.32	1.53
	90	8.17	1.59	0.54	0.39	0.12	0.26	1.41

Table 4 Elemental Concentrations Detected by APXS with Different Integration Times

	Integration time (min)	Mg	Al	Si	K	Ca	Ti	Fe
Elemental concentration (%)	10	4.68±1.17	7.40±0.35	19.45±0.31	1.65±0.02	10.27±0.04	1.44±0.01	8.47±0.32
	20	6.19±1.09	7.09±0.23	19.22±0.22	1.61±0.01	9.92±0.03	1.38±0.01	7.88±0.21
	30	5.38±0.78	7.12±0.19	19.25±0.18	1.63±0.01	10.11±0.02	1.41±0.01	8.52±0.18
	45	5.45±0.64	6.90±0.15	19.28±0.15	1.64±0.01	10.18±0.02	1.43±0.01	8.60±0.15
	60	5.23±0.53	6.97±0.13	19.29±0.13	1.65±0.01	10.23±0.02	1.43±0.00	8.69±0.13
	90	5.47±0.45	7.10±0.11	19.20±0.10	1.62±0.01	10.16±0.01	1.42±0.00	8.48±0.12
Statistical deviations (%)	10	13.33	16.54	8.3	10.00	6.2	5.88	2.42
	20	14.63	11.65	7.02	7.33	2.59	1.47	4.72
	30	0.37	12.13	7.18	8.67	4.55	3.68	3.02
	45	0.93	8.66	7.35	9.33	5.27	5.15	3.99
	60	3.15	9.76	7.41	10.00	5.79	5.15	5.08
	90	1.3	11.81	6.9	8.00	5.07	4.41	2.54

3.2 Results of Powder Samples with Different Working Distances

Figure 7 shows the channel counts data of powder samples with different integration times. Seven elements were identified from the spectrum, including Mg, Al, Si, K, Ca, Ti and Fe. We performed an iterative least-squares fit of a single Gaussian peak and calculated the area of each peak and its statistical deviation (Table 5).

Figure 8 shows that the peak area and its statistical deviation change with increasing working distance. We noted that the statistical deviations increase with working distance. The distance affected light elements (Mg, Al and Si) more significantly. This suggests that when APXS works on the Moon, the sensor head must be close to the target in order to obtain precise APXS results and it also helps the identification of light elements Mg, Al and Si.

According to Poisson statistics, the statistical deviation of total counts should be proportional to distance. The results of the statistical deviations of peak areas correlated with working distances shown in this plot deviate from an ideal linear relationship (Fig. 8). This indicates that there are other factors that affect the distance dependence on counts. In order to obtain reliable data, we employed the distance sensor in the front of the backup APXS sensor head from the CE-3 mission. The working distance (d) can be calculated based on the counting rate data in an in-situ detection model. Fu et al. (2014) describe an empirical, fourth-order polynomial relationship between the count rate and distance in detail. The polynomial fitting equation is expressed as follows (Fu et al. 2014): $d = (P_0 + P_1C + P_2C^2 + P_3C^3 + P_4C^4)$, where P_i is the parameter of the fourth-order

Table 5 Peak Areas and Their Statistical Deviations with Different Working Distances

	Working distance (mm)	Mg	Al	Si	K	Ca	Ti	Fe
Peak area (counts)	10	870	5997	29135	52176	455752	107570	9356
	20	590	4041	20056	36261	319341	75731	6177
	30	430	3014	14355	25618	223833	52399	4005
	40	358	2180	10614	18950	168041	39554	2974
	50	269	1694	7927	14160	126059	29646	2048
	70	95	1073	5089	9120	78817	18619	1378
	90	66	899	3486	6028	53539	12717	932
	110	34	488	2288	4364	38167	8953	614
Statistical deviations (%)	10	8.52	1.82	0.64	0.47	0.15	0.32	1.28
	20	10.98	2.27	0.78	0.57	0.18	0.38	1.66
	30	14.43	2.7	0.93	0.67	0.21	0.45	2.16
	40	15.8	3.4	1.11	0.8	0.25	0.53	2.59
	50	18.91	4.03	1.31	0.96	0.29	0.63	3.39
	70	53.37	5.62	1.7	1.24	0.36	0.8	4.69
	90	68.46	6.16	2.15	1.62	0.45	1	6.92
	110	129.7	10.08	2.89	1.96	0.53	1.23	9.87

Table 6 Elemental Concentrations Detected by APXS with Different Working Distances

	Working distance (mm)	Mg	Al	Si	K	Ca	Ti	Fe
Elemental concentration (%)	10	5.42±0.46	6.61±0.12	19.15±0.12	1.63±0.01	9.99±0.01	1.4±0.00	9.5±0.12
	20	5.38±0.59	6.51±0.15	19.23±0.15	1.65±0.01	10.19±0.02	1.44±0.01	9.27±0.15
	30	5.45±0.79	6.77±0.18	19.31±0.18	1.63±0.01	9.95±0.02	1.38±0.01	9.04±0.20
	40	6.06±0.96	6.62±0.23	19.22±0.21	1.62±0.01	10.02±0.03	1.4±0.01	8.56±0.22
	50	6.03±1.14	6.8±0.27	19.02±0.25	1.59±0.02	9.89±0.03	1.37±0.01	8.84±0.30
	70	/	6.78±0.38	19.26±0.33	1.62±0.02	9.76±0.04	1.36±0.01	7.99±0.37
	90	/	7.76±0.48	18.29±0.39	1.43±0.02	8.76±0.04	1.2±0.01	6.95±0.48
	110	/	7.86±0.79	17.8±0.51	1.54±0.03	9.45±0.05	1.3±0.02	7.07±0.70
Statistical deviations (%)	10	0.37	4.09	6.63	8.67	3.31	2.94	14.87
	20	0.37	2.52	7.07	10.00	5.38	5.88	12.09
	30	0.93	6.61	7.52	8.67	2.90	1.47	9.31
	40	12.22	4.25	7.02	8.00	3.62	2.94	3.51
	50	11.67	7.09	5.9	6.00	2.28	0.74	6.89
	70	/	6.77	7.24	8.00	0.93	0.00	3.39
	90	/	22.2	1.84	4.67	9.41	11.76	15.96
	110	/	23.78	0.89	2.67	2.28	4.41	14.51

polynomial fitting equation and C is the counting rate collected when the sensor head is positioned in the designated location.

Table 6 shows the elemental concentrations and their associated statistical deviations. We found that the working distance exhibits a different effect on these elements. The errors in Mg and Al concentrations increase with working distance. The Mg peak cannot be identified when the distance is more than 50 mm. However, the error in Si concentration decreases with working distance. Errors from other elements do not show any correlations with increasing working distance.

3.3 Comparison of Bulk Basalt and Standard Sample

Figure 9 shows the APXS spectra of bulk basalt. The working distance is 30 mm and integration time is 30 min. Table 7 shows the elemental concentrations of bulk basalt detected by APXS. Seven ele-

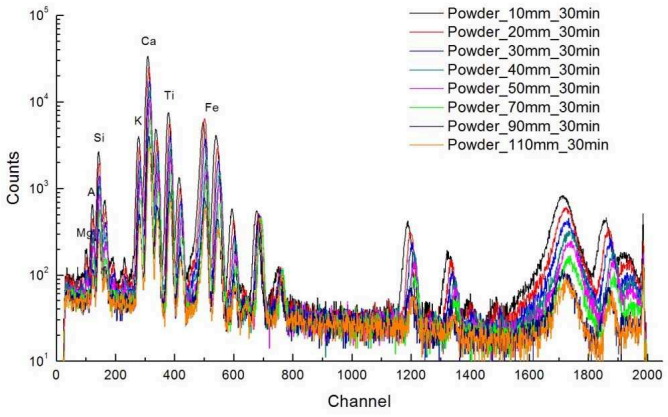

Fig. 7 APXS spectra of powder samples with different working distances.

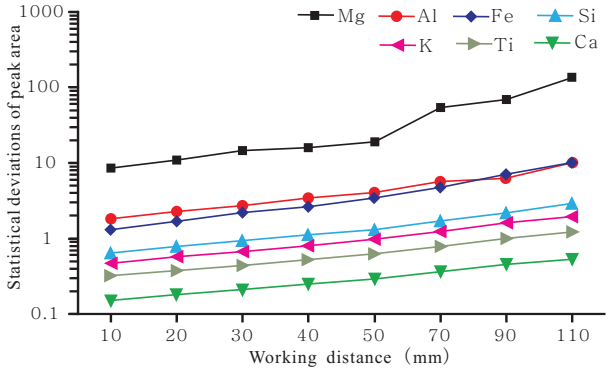

Fig. 8 The statistical deviations of peak areas correlated with working distances.

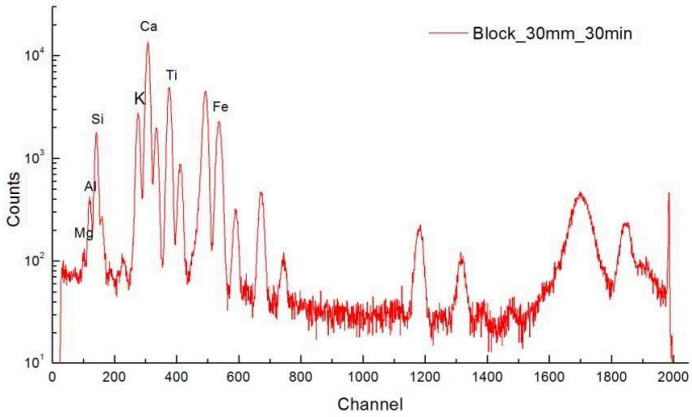

Fig. 9 APXS result of bulk basalt with a distance of 30 mm and integration time of 30 min.

Table 7 Elemental Concentrations of Bulk Basalt

	Mg	Al	Si	K	Ca	Ti	Fe
Peak area	484	4359	19638	36823	186832	71371	4709
Statistical deviation of APXS results (%)	13.01	2.2	0.79	0.57	0.24	0.39	2.48
Concentration (%)	4.8±0.62	8.06±0.18	21.26±0.17	1.95±0.01	6.91±0.02	1.46±0.01	8.5±0.21
Standard value (%)	5.5±0.04	7.1±0.02	20.58±0.03	1.7±0.02	6.56±0.03	1.55±0.01	9.57±0.04
Statistical deviation	12.70%	13.50%	3.30%	14.70%	5.30%	5.80%	11.20%

ments are identified, including Mg, Al, Si, K, Ca, Ti and Fe. Compared with chemical compositions analyzed by XRF in a laboratory, the statistical deviation of major elements is smaller than 15%.

4 CONCLUSIONS

In the present study, we tested the ability of the APXS to detect elements and investigated the effects of distance and time in measurements with the backup APXS instrument from the Yutu rover. The results indicate that APXS could detect seven major elements, including Mg, Al, Si, K, Ca, Ti and Fe, with a working distance of less than 30 mm and an integration time of 30 min. The analytical accuracy is better 15%. These tests verify the detection ability of the instrument for major elements in the sample. This study also compares the measurements with different working distances and integration times. The results suggest that an increase in integration time could reduce the measurement error of peak area, which helps in the detection of Mg, Al and Si. However, the increase in working distance could result in larger errors in measurement, which significantly influence the detection of element Mg. When the distance is more than 50 mm, APXS cannot detect the element Mg.

References

Campbell, J. L., Andrushenko, S. M., Taylor, S. M., & Maxwell, J. A. 2010, Journal of Geophysical Research (Planets), 115, 4009

Economou, T. 2001, Radiation Physics and Chemistry, 61, 191

Economou, T. 2011, History of Applications of Radioactive Sources in Analytical Instruments for Planetary Exploration. Radioisotopes-Applications in Physical Sciences, ed. N. Singh, 155

Fu, X.-H., Li, C.-L., Zhang, G.-L., et al. 2014, RAA (Research in Astronomy and Astrophysics), 14, 1595

Gellert, R., Rieder, R., Brückner, J., et al. 2006, Journal of Geophysical Research (Planets), 111, 2

He, Z.-P., Wang, B.-Y., Lu, C., et al. 2014, RAA (Research in Astronomy and Astrophysics), 14, 1567

Ip, W.-H., Yan, J., Li, C.-L., et al. 2014, RAA (Research in Astronomy and Astrophysics), 14, 1511

Ji, A., Tao, G. Y., Zhuo, S. J., & Luo, L. Q. 2005, X-Ray Fluorescence Spectrometry Analysis (in Chinese) (Beijing: Science Press)

Li, C.-L., Mu, L.- L., Zou, X.-D., et al. 2014, RAA (Research in Astronomy and Astrophysics), 14, 1514

Liang, X. H., Wu, M. Y., Wang, H. Y., et al. 2013, Spectroscopy and Spectral Analysis (in Chinese), 33, 1360

Liu, B., Li C.-L., Zhang, G.-L., et al. 2014a, RAA (Research in Astronomy and Astrophysics), 14, 1578

Liu, J.-J., Yan, W., Li, C.-L., et al. 2014b, RAA (Research in Astronomy and Astrophysics), 14, 1530

Peng, W. X., Wang, H. Y., Cui, X. Z., et al. 2014, in Lunar and Planetary Science Conference, 45, 1699

Ren, X., Li C.-L., Liu, J.-J., et al. 2014, RAA (Research in Astronomy and Astrophysics), 14, 1557

Rieder, R., Gellert, R., Brückner, J., et al. 2003, Journal of Geophysical Research (Planets), 108, 8066

Tan, X., Liu, J.-J., Li, C.-L., et al. 2014, RAA (Research in Astronomy and Astrophysics), 14, 1682

Wu, M. Y., Wang, H. Y., Peng, W. X., et al. 2012, Spectroscopy and Spectral Analysis (in Chinese), 32, 1965